Journal of Sol-Gel Science and Technology
https://doi.org/10.1007/s10971-024-06539-x

ORIGINAL PAPER

Effect of Al on photoluminescence properties of Nd^{3+} in silicate glass prepared by in-situ sol-gel method

K. M. S. Dawngliana[1] · Lalruat Puia[1] · A. L. Fanai[2] · Ralte Lalrempuia[3] · S. Rai[1]

Received: 2 November 2023 / Accepted: 29 August 2024

Abstract

This article discusses our investigations into the structural and spectroscopic properties of Nd^{3+} co-doped alumino-silicate glass prepared by an in-situ sol-gel method. Structural characterization was carried out using X-ray powder diffraction (XRD), Fourier-transform infrared spectroscopy (FTIR) and scanning electron microscopy (SEM) techniques. The XRD analysis reveals that the material is still amorphous even after being heated to 900 °C. FTIR analysis was used to identify the functional groups of the produced sol-gel silicate glass. The optical absorption spectra from the ground state $^4I_{9/2}$ show seven peaks in the UV-VIS and NIR regions. The optical absorption spectrum of Nd^{3+} co-doped alumino-silicate glass-ceramic was used to determine the Judd-Ofelt (JO) intensity parameters (Ω_2, Ω_4 and Ω_6). The photoluminescence (PL) spectrum was recorded with a 2W diode laser source of 808 nm excitations. From the larger stimulated emission cross-section (3.80 x 10^{-20} cm^2) of the $^4F_{3/2} \rightarrow {}^4I_{11/2}$ transition, it is concluded that the SiNdAl glasses could be highly useful for the development of solid state laser materials. From the observed refractive indices at three different wavelengths, non-linear parameters for the glass, such as the Abbe number (υ_{Ab}) and non-linear refractive index (n_2), are derived.

Graphical Abstract

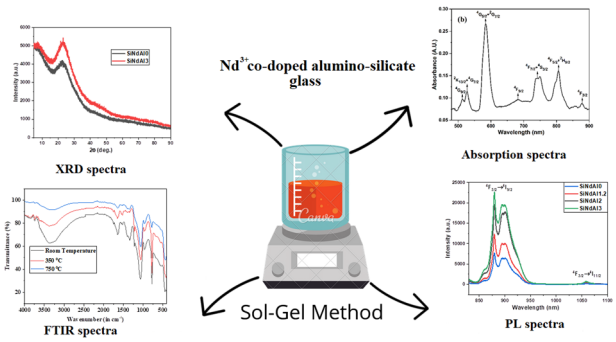

Keywords Sol-gel · Neodymium · Aluminum · Photoluminescence

✉ K. M. S. Dawngliana
jerrykms0000@gmail.com

[1] Laser and Photonics Laboratory, Department of Physics, Mizoram University, Aizawl 796004, India

[2] Physic Section, Mahila Mahavidyalaya, Banaras Hindu University, Varanasi 221005, India

[3] Department of Chemistry, Mizoram University, Aizawl 796004, India

Published online: 09 September 2024

Highlights

- Nd^{3+} ions co-doped with alumino-silicate glass is prepared by in-situ sol-gel methods.
- Red-shift in absorption peaks observed after annealing due to nephelauxetic effect. The Judd–Ofelt parameter Ω_2 increased and Ω_6 decreased with annealing.
- PL intensity increases with annealing. PL intensity increases with increasing Al content.
- Various physical parameters like density, refractive index and non-linear polarizability are measured to investigate possible device applications of the samples.

1 Introduction

Recently, the study of rare earth (RE) ions doped amorphous or crystalline solids materials have attracted much attention because of their attractive optical characteristics, high transition temperature, and low thermal expansion coefficients [1–3]. These materials hold promise for diverse applications such as optical communications, biosensors, optical amplifiers, and light-emitting diodes (LEDs) [4, 5]. Rare earth-doped materials are essential components for low-cost integrated laser sources, integrated optical amplifiers, 3D display devices, sensors, up-conversion fibers, and low-loss components [6–8], among other current optical technology products [8, 9], because of their fluorescence in the near IR region at 1.06 μm after the introduction of the first glass laser by Snitzer [10]. The choice of a suitable glass matrix as a host for the development of efficient optical devices doped with lanthanide ions is an active area of research. Even hosts with higher phonon energies can exhibit fluorescence spectra effectively due to the relatively large energy gap in the transition from the lanthanide ion's $^4F_{3/2}$ level to the next lower $^4I_{15/2}$ level [9]. SiO_2 glass is an excellent host for lanthanide ions because of its low cost, high optical transmission, low thermal expansion, excellent chemical and thermal stability, good mechanical strength and good moisture resistance [11]. However, the exceptional thermal stability of SiO_2 glass poses challenges in conventional synthesis methods, as silica typically required processing temperatures above 2000 °C [12]. Such doped silica glasses can be created using the sol-gel process at significantly lower temperatures. Additionally, while still preserving an amorphous character, it allows the incorporation of larger dopant concentrations than traditional melt glasses [13, 14]. However, a variety of factors prevent them from being used as effective optical materials. In the sol-gel glass hosts, lanthanide ions tend to cluster, which causes concentration quenching [15]. Additionally, there is quenching brought on by hydroxyl (-OH) groups that were left over from the initial preparation procedure. Prolonged heat treatment can lower the hydroxyl concentration. Heating affects the physical parameters of the system, such as density, refractive index, and other structural aspects, in addition to removing hydroxyls [16, 17]. Vibrations within the host glass provide a non-radiative relaxation path for excited ions, resulting in energy loss via phonon in the glass network [18]. SiO_2 glass has a rather high maximum phonon energy (1100 cm^{-1}) and energy loss occurs via multi-phonon relaxation [19]. Hence, photoluminescence (PL) is typically only observed from excited states with significant energy gaps. Additionally, the energy level structure of the lanthanide ions makes it susceptible to cross-relaxation as concentration increases, which tends to result in Nd^{3+} clustering. It has been demonstrated that co-doping aluminum with lanthanide ions in doped sol-gel glasses increases fluorescence output [20, 21]. Non-bridging oxygen's (NBOs) are believed to be introduced into the matrix by aluminum doping [22]. With silicon or aluminum, the NBOs only form one bond, leaving another open to form a bond with the lanthanide ions. Al species surround each lanthanide ions in this way, separating them from one another. Hence, cross-relaxation is decreased and PL efficiency is raised.

The highly efficient $^4F_{3/2} \rightarrow {}^4I_{11/2}$ lasing transition occurring at 1058 nm positions Nd^{3+} as one of the most extensively studied RE^{3+} ions when combined with various hosts, particularly for its application in solid-state lasers. The presence of absorption bands across the UV-VIS-NIR spectrum further enhance its suitability, facilitating the pumping of the Nd-laser systems through either broad-band sources such as xenon lamps or diode lasers [10, 20]. Laser efficiency primarily relies upon factors like emission cross-section and luminescence decay rates, which are significantly influenced by non-radiative decays within the system, including multi-phonon relaxation processes [9, 10]. In hosts derived from sol-gel techniques, the phenomenon of dopant clustering where luminescent species aggregate through oxygen linkage can lead to a reduction in luminescence intensity due to cross-relaxation and energy transfer processes [20]. However, these limitation can be mitigated to a considerable extent by incorporating small quantities of co-dopant like Al, TiO_2, borate and tellurite [1, 2, 6, 9], as well as utilizing organic salts as glass precursors instead of mineral acid salts, in addition to optimizing the concentrations of RE^{3+} ions and hosts.

We describe in this paper the physical, structural and optical properties of $(99\text{-}x)SiO_2 + 1NdF_3 + xAl_2O_3$ (here x = 0.0, 1.2, 2.0 and 3.0 mol%)(i.e. SiNdAl0, SiNdAl1.2, SiNdAl2 and SiNdAl3) prepared by using a sol-gel

technique. The structure of the as-prepared samples was examined using Fourier-transform infrared spectroscopy (FTIR) and X-ray powder diffraction (XRD). A potential process involved in the development of platelet morphology has been proposed based on the examination of the scanning electron microscopy (SEM) images. Using the optical absorption and fluorescence spectra, the spectroscopic parameters of the nanocrystals, such as radiative transition probability and branching ratio, were qualitatively analyzed and discussed. To verify the usefulness of the created glass samples, the physical properties are also measured.

2 Experimental

2.1 Precursor

All chemicals used in this study were of analytical grade and were used without further purification. Aluminum nitrate nona-hydrate ($Al(NO_3)_3{\cdot}9H_2O$, Merck, 99.5%), tetraethyl orthosilicate (TEOS; Sigma-Aldrich 99%), neodymium (III) fluoride (NdF_3, Sigma-Aldrich 99.99%), methanol (MeOH; Merck, 99.8%), nitric acid (HNO_3; Sigma-Aldrich 70%) and banana trunk sap were purchased and used as received.

2.2 Samples preparation synthesis of Nd^{3+} co-doped Al samples

The composition of the bulk glasses (in mol%) $(99\text{-}x)SiO_2 + 1NdF_3 + xAl_2O_3$ (here x = 0.0, 1.2, 2.0 and 3.0 mol%) were prepared by using a sol-gel technique with TEOS as the main precursor, methanol (CH_3OH) as the solvent, nitric acid (HNO_3) as the catalyst, and $Al(NO_3)_3{\cdot}9H_2O$ and NdF_3 as the source of dopants. For specific concentrations of Nd^{3+} and Al^{3+} dopant in a particular sample, the required amounts of NdF_3 and $Al(NO_3)_3{\cdot}9H_2O$ were dissolved in a mixture of methanol, nitric acid and banana trunk sap (a natural product containing more than 90% of water) and stirred for 50 min using a magnetic stirrer. TEOS was then added dropwise, and the resulting mixture was stirred for 2 h [23]. The final solutions contained TEOS, banana trunk sap, methanol, and HNO_3 in the following molar ratios: 1: 5.5: 3.5: 0.1. The final sol is then transferred to a plastic vessel sealed to prevent evaporation. After the sol has gelled and been sealed at room temperature for 26 days, some pinholes were made in a plastic container's lid to allow for slow evaporation. After that, the container was left standing for a few weeks. To make dense glass samples in the shape of discs, the gels were further dried in an electric muffle furnace by gradually heating to 40 °C and then annealing up to 1060 °C at a heating rate of 1 °C min^{-1}.

2.3 Techniques of characterization

Optical properties were recorded using a Horiba iHR320 imaging spectrometer. Optical absorption and photoluminescence spectra were recorded in the UV-VIS & NIR regions at room temperature (RT). The photoluminescence studies make use of an 808 nm diode laser source. X-ray diffraction (XRD, Empyrean, PANanalytical), using CuKα (λ_{ex}= 1.54Å) radiation, was used to determine the phase compositions of the powders. FTIR spectra were acquired with a IRAffinity-1S (SHIMADZU). Using the Archimedes principle and xylene as an immersion liquid, glass densities were calculated. An Abbe refractometer with a coating of monobromonaphthalene (C10H7Br) was used to determine the transparent glass' refractive index with an accuracy of (n ± 0.001). All measurements were performed at room temperature.

3 Result and discussions

3.1 X-ray powder diffraction studies

The powder X-ray diffraction spectrum of SiNdAl0 and SiNdAl3 in sol-gel glasses after annealing at 900 °C is shown in Fig. 1. Instead of sharp crystalline peaks, distinct broad peaks are seen, confirming the glass samples' glassy amorphous nature. The amorphous nature of silica glass is thought to be responsible for the broad peak at 2θ = 22 [23].

3.2 FTIR analysis

FTIR spectra of SiNdAl3 of glasses is annealed at different temperatures (room temperature, 350, and 750 °C), are

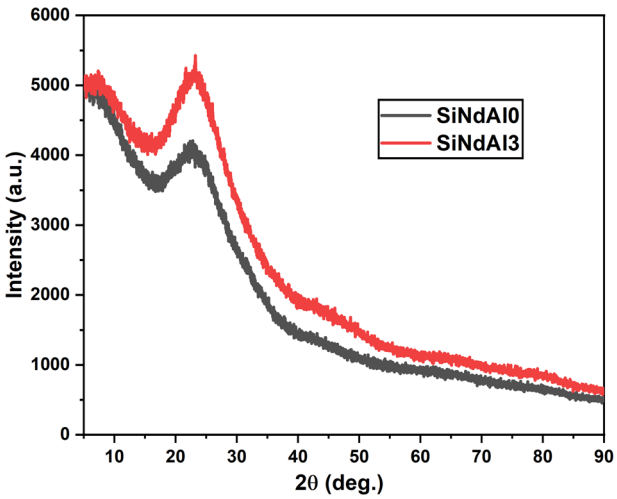

Fig. 1 XRD powder patterns of SiNdAl0 and SiNdAl3 in sol-gel glasses

shown in Fig. 2, in the 400–4000 cm^{-1} wavenumber range, while the corresponding band assignments are given in Table 1. A number of peaks can clearly be seen at about 417, 441, 471, 588, 671, 771, 964, 1065, 1219, 1335, 1397, and 3363 cm^{-1}. To create a 3-D silica network, TEOS is hydrolyzed and condensed with the help of water and alcohol. This process also yields Si-OH groups. The gel stage of the sol-gel glass consists mostly of water and other organic species. As the sintering temperature is increased, the broad peak between 3363 and 3723 cm^{-1} vanishes as a result of the removal of OH- and water molecules (H_2O), which are responsible for the sample's O-H stretching vibration [24]. The band's intensity is greatest for glass at room temperature and gradually decreases as the temperature rises. As temperatures increased, the peak associated with stretching of Si-OH bands and the appearance of absorbed water became less intense, according to the FTIR spectra [24]. The peak's broadening and shift to the low wavenumber side indicate a decrease in phonon energy. The aluminum ion modifies the network by creating non-bridging Al-O groups, such as Si-O-Al, which can also coordinate with lanthanide ions [25]. When the Si-O-Si bond breaks, the NBO of Nd-O-Si may also form [25]. Octahedrally coordinated Al(III)is associated with the bending mode around 487–548 cm^{-1}. Si-OH group polymerization results in Si-O-Si bonds with wavenumber of 1335–1397 cm^{-1} and 1057–1065 cm^{-1}, respectively [26]. The intensity of the Si-OH peak at 964 cm^{-1} decrease with increasing annealing temperature. Hence, annealing of the glass sample leads the components to gradually vanish from the glass host matrix, leading to the development of a stiff glassy network, which is evident from the FTIR spectra.

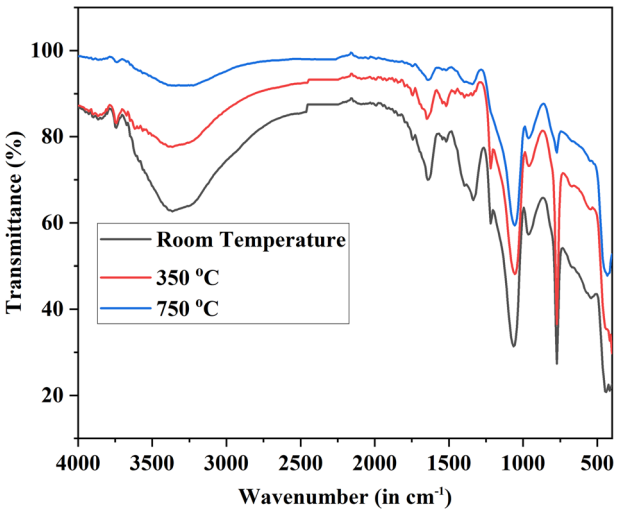

Fig. 2 The FTIR spectra of SiNdAl3 samples after being annealed at various temperatures

3.3 Characteristic physical properties

Selected physical properties of SiNdAl0, SiNdAl1.2, SiNdAl2, and are shown in Table 2. These values were obtained as outlined in our earlier research [27].

The variations in the sol-gel glasses' density (g/cm^3), refractive index, average molecular weight (M_T), inter ionic distance (R_i), and field strength ($x10^{13}$ cm^{-2}) as a function of Al content are shown in Fig. 3a, b [27]. The tendency of decreasing inter ionic distance in these glasses shows that the atoms are becoming more densely packed as the Al^{3+} ion concentration in the glasses increases [27]. Figure 3a

Table 1 The various assignments of the glass samples' FTIR peak positions

Wavenumber (cm^{-1})	Assignment	Observed intensity	Change in intensity during heating
417-441	Si-O and O-Si-O vibrations caused by antisymmetric stretching [26]	Broad	At room temperature and 350 °C, there are two peaks at 417 and 439 cm^{-1}. At 750 °C, a peak emerges at 428 cm^{-1}.
487–548	Si-O-Al bending with an antisymmetric NBO (Non-bridging oxygen) [25]	Minor peak	Intense peak observed at room temperature and 350 °C; not observed for sample heated at 750 °C
673	Bending of the symmetric Si-O of SiO_4 [25]	Minor peak	Minor peak at room temperature and 350 °C; intensity decreases with rising temperature
771	Si-OH stretching [54]	Strong	Decreases with increasing temperature
964	Si-O-H stretch vibrational mode	Strong	Decreases with increasing temperature
1057–1065	Si-O-Al & Al–O–Al antisymmetric stretching [25]	Intense peak	Reduction in intensity and a red shift with increasing temperature
1219	Stretching vibration C-O-C [33]	Minor peak	Peak not observed when T >750 °C
1335–1397	C-O-H stretching [33]	Broad	Decreases with increasing temperature
1519-1652	–OH bending vibration mode of water	Minor peak	Decreases with increasing temperature
3363-3723	O-H stretching [55]	Broad, strong	Decreases with increasing temperature

Table 2 Selected physical properties of SiNdAl0, SiNdAl1.2, SiNdAl2 and SiNdAl3 annealed at 1060 °C

Physical properties	SiNdAl0	SiNdAl1.2	SiNdAl2	SiNdAl3
Refractive index (n)	1.465	1.589	1.613	1.674
Density (ρ) (gm/cm^3)	1.921	2.06	2.11	2.20
Thickness (Z) (cm)	0.179	0.178	0.177	0.178
Radius (cm)	1.214	1.215	1.213	1.214
Average molecular weight (M_T) (g)	65.665	72.163	74.085	77.982
Reflection losses (R_L) (%)	0.036	0.052	0.055	0.064
Molar refractivity (R_m) (cm^{-3})	9.449	11.806	12.223	13.302
Energy gap (E_g)	10.48	8.78	8.5	7.82
Molar electronic polarizability (α_m)	3.676	4.685	4.694	5.006
Dielectric constant (ϵ)	2.146	2.525	2.602	2.802
Optical dielectric constant(ϵ-1)	1.146	1.525	1.602	1.802
Electronic polarizability (α_e) (x 10^{-25})	1.096	1.337	1.381	1.488
Nd^{3+} ion concentration (N)(x10^{22} $ions/cm^3$)	0.141	0.429	1.771	5.258
Molar volume (V_m) (cm^3/mol)	34.183	35.031	35.111	35.446
Polaron radius(R_p)(x10^{-8})Å	14.92	11.51	7.18	4.35
Inter-ionic distance (R_i) (x10^{-7})Å	4.139	2.857	1.781	1.239
Field strength (F)(x $10^{13}cm^{-2}$)	0.804	1.570	4.209	12.102
Metallization criterion (M)	0.724	0.663	0.652	0.625

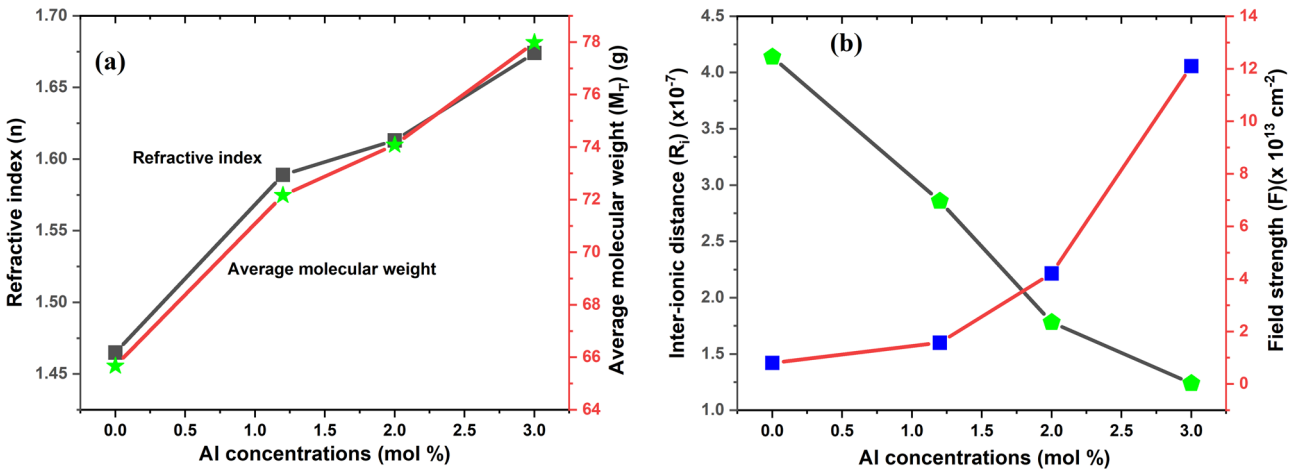

Fig. 3 **a** Variations in the refractive index and average molecular weight for SiNdAl0, SiNdAl.2, SiNdAl2, and SiNdAl3. **b** Inter ionic distance (10^{-7}) and field strength (10^{13} cm^{-2}) parameter variations in sol-gel glasses as a function of Al content

shows that the refractive index of SiNdAl in sol-gel glasses rises as the concentration of dopant ions increases. As the density of the SiNdAl in sol-gel glasses rises along with the concentration of the dopant ions, the medium's refractive index will rise as well. It is also evident from Fig. 3b that the field strength values rise as the concentration of Al^{3+} ions does. This is clear from the fact that when the concentration of aluminum ions in glass rises, more ions will be made available per unit volume, increasing the field strength. The electronic polarizability of these glasses is of the order 10^{-25}, which is surprisingly low [27], as shown in Table 2.

3.4 Absorption spectra

The absorption spectra of SiNdAl3 following annealing at 150 or 1060 °C are shown in Fig. 4a, b, respectively. The relative intensities of the various absorption peaks shift as the heat treatment is varied, leading to associated changes in the physical characteristics of the material. The low-temperature sample quickly reabsorbs atmospheric moisture because it is extremely porous, has a low density of about 1.34 g/cm^3, and is exposed to the atmosphere. The sample loses the majority of its porosity after being annealed at 1060 °C and reaches a density of

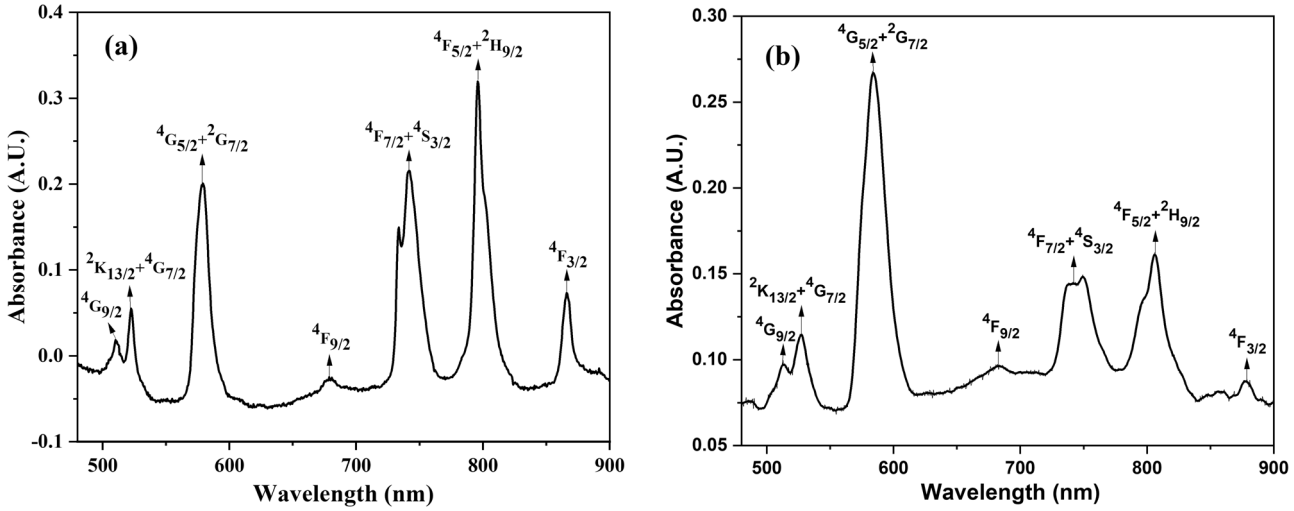

Fig. 4 Absorbance spectra of SiNdAl3 after annealing at (**a**) 150 and (**b**) 1060 °C

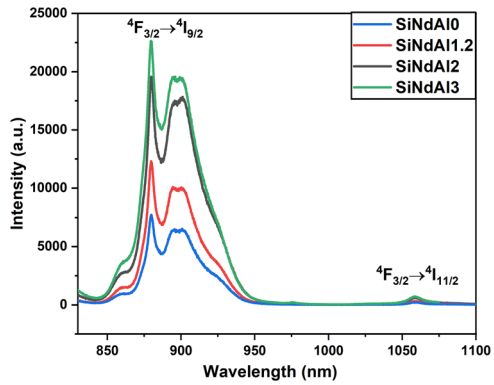

Fig. 5 PL spectra of SiNdAl0, SiNdAl1.2, SiNdAl2 and SiNdAl3 after annealing at 1060 °C

around 2.32 g/cm^3 which is comparable to melt glass. As seen in Fig. 4, there are seven bands in the absorption spectra that correspond to the transitions between the ground state (GS) $^4I_{9/2}$ and the excited states (ES) of the 4f^3 configuration of lanthanide ions [23]. The band at 512, 523, 579, 679, 742, 795 and 870 nm correspond to the transitions from the $^4I_{9/2}$ → level to $^4G_{9/2}$, $^2K_{13/2}$ + $^4G_{7/2}$, $^4G_{5/2}$ + $^2G_{7/2}$, $^4F_{9/2}$, $^4F_{7/2}$ + $^4S_{3/2}$, $^4F_{5/2}$ + $^2H_{9/2}$ and $^4F_{3/2}$ respectively [28]. One transition in particular, $^4I_{9/2}$ → $^4G_{5/2}$ + $^2G_{7/2}$, is more intense than others in the dense glass and has high oscillator strengths across all the glasses being studied. [28]. The selection rules $|\Delta J| \leq 2$; $|\Delta L| \leq 2$ and $|\Delta S| = 0$ are valid for this transition, which is also referred to as a hypersensitive transition [28]. As the material is heated to higher temperatures, the redshift in the absorption peaks that occurs is another interesting result. In Fig. 4a, b, the major near-infrared peaks shift from 795 nm and 871 nm to 806 nm and 879 nm [29]. The redshift seen after annealing is caused by the nephelauxetic effect, which occurs as the Nd^{3+} starts becoming incorporate into the covalent glass network [29].

Table 3 Stark splitting in the spectra of SiNdAl0, SiNdAl1.2, SiNdAl2 and SiNdAl3 annealed at 1060 °C

Transitions $^4G_{5/2}$ →	Wavelength (λ_P) (nm)	Energy (cm^{-1})	ΔE
$^4I_{9/2}$	879	11376	0
	894	11185	191
	901	11098	278
	926	10799	577

3.5 Photoluminescence spectra

The photoluminescence spectra of SiNdAl0, SiNdAl1.2, SiNdAl2 and SiNdAl3 glasses annealed at 1060 °C, were recorded using an excitation wavelength of λ_{ex} = 808 nm in the 830–1100 nm range as shown in Fig. 5. Two broad, asymmetric bands in the emission spectra are located around 879 and 1058 nm. These emission bands correspond to the RE^{3+} ion transitions $^4F_{3/2}$ → $^4I_{9/2}$ and $^4F_{3/2}$ → $^4I_{11/2}$, respectively. With increasing concentrations of aluminum ions and an associated decrease in concentration quenching, an increase in the intensity of a broad peak at about 1058 nm may be seen [29]. The most intense transition gives rise to a peak at 879 nm, with increasing Al^{3+} concentration leading to an associated increase in the emission intensity [30, 31] The increase in NBO changes the electronic structure of glasses, promoting transitions with lower energy [25]. In silicate sol-gel glasses, it has been reported that SiNdAl0, SiNdAl1.2, SiNdAl2 and SiNdAl3 results in PL spectra with splitting (Stark splitting), which is consistent with the host being altered by the presence of Al (Table 3) [32].

3.6 Effect of annealing temperature of PL intensity

Using an excitation wavelength of 808 nm, the photoluminescence spectra of SiNdAl3 sol-gel glasses was measured at various annealing temperatures. NBO (Si-O-Al), whose phonon energy is lower than that of the Si-O-Si bond, is formed and causes asymmetry [25]. This is confirmed by the observed FTIR spectra. The sample quenched by the hydroxyl (OH) group after being annealed at 650 °C exhibits low PL intensity, since the OH group quenches the PL of Nd^{3+} ions [29]. Energy transfer to the Nd^{3+} ions in silica xerogel is inhibited by the creation of electrons and holes through defect recombination. As a result, the elimination of the OH group increases the PL intensity for glasses that are annealed at higher temperatures (Fig. 6) [29]. As a result, PL enhancement is due to host matrix asymmetry and OH group elimination at high annealing temperatures. Stark splitting at the Nd^{3+} $^4I_{9/2}$ transitions in the glass is observed in the photoluminescence spectra of SiNdAl0, SiNdAl1.2, SiNdAl2 and SiNdAl3 (Table 3), which is consistent with the host being modified at the higher temperature (1060 °C) [33]. A comparison of the stark-split energy levels of Nd^{3+} in various crystalline lattices is included in Table 4.

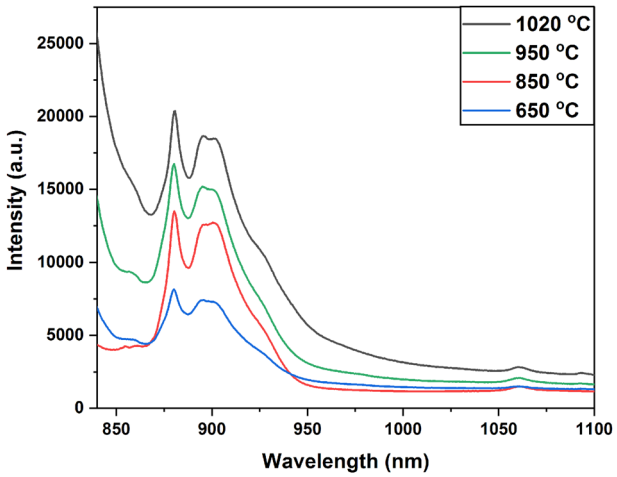

Fig. 6 PL spectra of SiNdAl3 glass samples annealed at different temperatures

Table 4 Comparison of stark-split energy levels of Nd^{3+} in various crystalline lattices

Transitions $^4G_{5/2}$ →	Nd^{3+} in YAG [53] (cm^{-1})	Nd^{3+} in Nd_2O_3 [56] (cm^{-1})	Present work (cm^{-1})
$^4I_{9/2}$	0	0	0
	133	115	191
	199	123	278
	310	238	577
	859	249	-

For the cross-relaxation of two ions that are close to one another, the energy level structure of Nd^{3+} provides a very effective pathway [30]. With increasing concentration, the possibility of cross-relaxation increases because Nd^{3+} clusters are more likely to form. Both Nd^{3+} ions may occupy the intermediate $^4I_{15/2}$ state before relaxing non-radiatively to the ground state as a result of one RE ion in the excited $^4F_{3/2}$ state transferring some of its energy to the neighboring ion in the ground state (Fig. 7) [29].

3.7 Oscillator strength-Judd-Ofelt analysis

As the ions around the RE have an impact on the transition probabilities between 4f states, it is essential to understand a number of spectroscopic factors while designing a suitable RE doped glass [34]. Typically, the Judd-Ofelt (JO) theory [35, 36] is used to approximate the transition probabilities

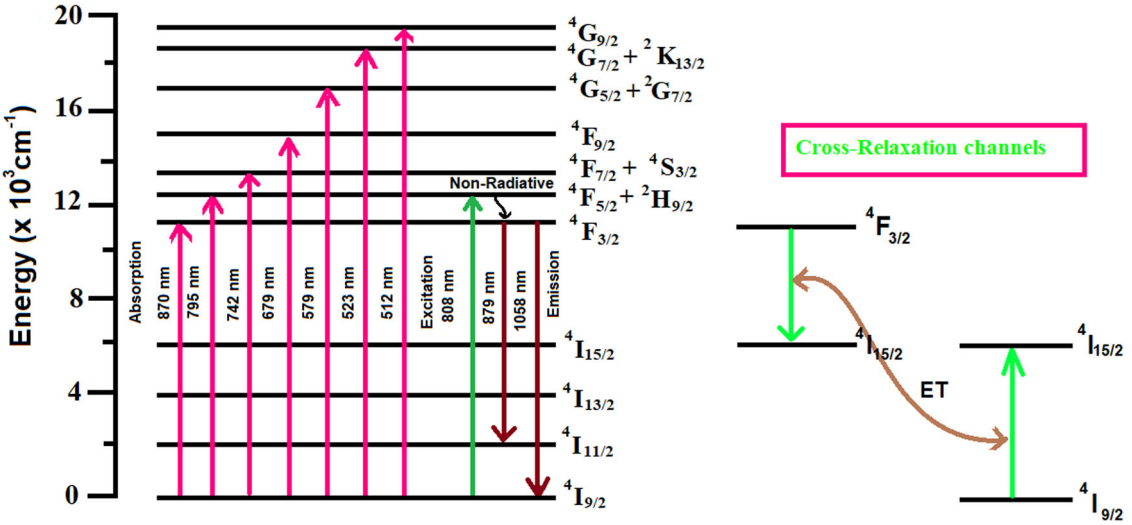

Fig. 7 Schematics diagram of energy level of Nd^{3+} in SiNdAl0, SiNdAl1.2, SiNdAl2 and SiNdAl3

using data on the absorption spectra of various f-f transitions. Using J-O theory, the calculated oscillator strengths (f_{cal}) for the f-f transitions of RE ions from their GS $|\Psi J\rangle$ to the ES $|\Psi' J'\rangle$ may be written as,

$$f_{cal}^{ed} = \frac{8\pi^2 m_e c\overline{\upsilon}(n^2+2)^2}{3h(2J+1)9n}\Sigma_{\lambda=2,4,6}\Omega_\lambda(\Psi J||U^\lambda||\Psi' J')^2 \qquad (1)$$

where the J-O intensity parameters, on which the oscillator strength depends, are Ω_λ for $\lambda = 2$, 4, and 6. Planck's constant, electron mass, refractive index, speed of light in a vacuum, and average transition wavelength are all represented in Eq. (1) by m_e, n, c, and h, respectively, whereas J is the initial transition states of the total angular momentum quantum number. In this calculation, the host independent RME values, $\|U^\lambda\|$, as obtained by Carnal et al. [37], are employed. For $\lambda = 2$, 4, and 6, the reduced unit tensor operators are $\|U\lambda\|$, and the remaining symbols have their normal meanings. The following formula is used to correlate the measured oscillator strengths (f_{exp}) of the observed bands,

$$f_{exp} = 4.319 \times 10^{-9}\int \varepsilon(\nu)d\upsilon \qquad (2)$$

where $\varepsilon(\nu)$ is the molar absorptivity at frequency in cm^{-1}. The forced electronic dipole transitions "solution to the correlation matrix" is derived with the help of MATLAB (MATLABR12) commands [38]. Least square fit analysis is used to calculate the three J-O intensity parameters. An approximate method of intermediate coupling is used to determine the reduced unit tensor operators [38]. Values of $\|U^\lambda\|$ for Nd^{3+} ions according to Carnall et al. [39], which are independent of hosts for these operators, are used in these calculations and the index of refraction, $n = 1.478$ (porous glass), and $n = 1.674$ (dense glass) of SiNdAl3 were both utilized.

The JO intensity parameters are in the order $\Omega_6 > \Omega_2 > \Omega_4$ (in porous glass) and $\Omega_2 > \Omega_4 > \Omega_6$ (in dense glass). The large number of Ω_6 reasonably indicates that the hosts [Nd-O, Nd-Al] [40–42] and Nd^{3+} ions have covalent bonds with the other two metals. The Ω_2 value in the present study increases from 2.12×10^{-20} cm^2 in the sample treated at lower temperature to 4.93×10^{-20} cm^2 for the high-temperature sample, while the corresponding Ω_6 value decreases from 3.32×10^{-20} cm^2 to 2.21×10^{-20} cm^2. This might be because as the temperature increases, more Nd^{3+} ions are incorporated into the strong covalent glass network and hydroxyl ions are removed. A reduced centrosymmetric coordination environment around Nd^{3+} ions in the silica host is also suggested by the large value of Ω_2. Although the JO analysis and the Ω_λ parameters [43] have a significant inherent error, a pattern is seen where the Ω_2 value rises as the sample processing temperature rises (Table 5a, b). Similar patterns were seen in the emission spectra of the RE^{3+} ion in sol-gel glass by Qiao et al. [44] and Reisfeld et al. [45], both of which showed that Al may reduce the site symmetry of the RE^{3+} ion. Due to the bond between the ligand atoms and RE^{3+} ions, the values of Ω_4 and Ω_6 produce vibronic transitions, which are dependent on the dielectric and viscosity characteristics of the medium (glass) [46]. Table 6

Table 5 **a** Oscillator strengths and Ω_λ parameters for SiNdAl3 samples in the porous gel stage processed at 150 °C; **b** Oscillator strengths and Ω_λ parameters for SiNdAl3 samples annealed at 1060 °C

Transitions $^4I_{9/2}$→ES	Energy (cm^{-1})	Wavelength (nm)	f_{exp} (x 10^{-6})	f_{cal} (x 10^{-6})
(a)				
$^4G_{9/2}$	19531	512	1.02	1.45
$^2K_{13/2} + {}^4G_{7/2}$	19120	523	2.46	4.70
$^4G_{5/2} + {}^2G_{7/2}$	17271	579	9.98	3.30
$^4F_{9/2}$	14728	679	2.68	0.37
$^4F_{7/2} + {}^4S_{3/2}$	13477	742	5.42	11.39
$^4F_{5/2} + {}^2H_{9/2}$	12579	795	4.09	2.53
$^4F_{3/2}$	11494	870	1.56	0.66
	$\Omega_2 = 2.12$ (x 10^{-20} cm^2)	$\Omega_4 = 2.09$ (x 10^{-20} cm^2)	$\Omega_6 = 3.32$ (x $10^{-20}cm^2$)	
		$\Omega_4/\Omega_6 = 0.63$ (x 10^{-20})		
(b)				
$^4G_{9/2}$	19268	519	0.78	1.28
$^2K_{13/2} + {}^4G_{7/2}$	18797	532	3.12	3.25
$^4G_{5/2} + {}^2G_{7/2}$	17123	584	18.96	11.95
$^4F_{9/2}$	14641	683	2.08	0.86
$^4F_{7/2} + {}^4S_{3/2}$	13316	751	3.70	4.87
$^4F_{5/2} + {}^2H_{9/2}$	12422	805	3.72	3.96
$^4F_{3/2}$	11390	878	1.60	0.95
	$\Omega_2 = 4.93$ (x 10^{-20} cm^2)	$\Omega_4 = 3.01$ (x 10^{-20} cm^2)	$\Omega_6 = 2.21$ (x $10^{-20}cm^2$)	
		$\Omega_4/\Omega_6 = 1.36$ (x 10^{-20})		

Table 6 Spectroscopic quality factor ($X=\Omega_4/\Omega_6$) and JO parameters (x 10^{-20} cm^2) comparison of the Nd^{3+} co-doped with aluminum in SiO_2 glasses with previous published works

Ω_2	Ω_4	Ω_6	Ω_4/Ω_6	References
2.12	2.09	3.32	0.63	Present work (150 °C)
4.93	3.01	2.21	1.36	Present work (1060 °C)
7.16	3.20	2.97	1.077	$^{SiO}2$-Al3+:Nd3+ [57]
2.088	2.260	2.884	0.795	$^{NdCl}3$ in methanol [58]
1.790	1.542	1.756	0.878	$^{NdCl}3$ in butanol [58]
1.039	1.531	3.209	0.447	$^{NdCl}3$ in iso-propanol [58]
0.10	3.58	2.87	1.24	Glass A [59]
0.09	3.68	2.94	1.25	Glass B [59]
2.14	2.57	1.93	1.33	BSGdCaNd0.5 [60]
1.83	4.73	4.19	1.09	Fluorophosphates [61]
4.81	1.97	3.94	0.50	SPB1 [62]

Table 7 Radiative lifetimes (τ_R), branching ratios (β_r (%)), total transition probabilities (A_{ed}), radiative transition probabilities (A_T), effective bandwidth ($\Delta\lambda_{eff}$) and emission cross-section ($\sigma_P(\lambda_P)$) for SiNdAl3 glass annealed at 1060 °C

Transitions $^4F_{3/2} \rightarrow$	Energy (in cm^{-1})	A_{ed} (in s^{-1})	β_r (in %)	$\Delta\lambda_{eff}$ (nm)	$\sigma_P(\lambda_P)$ (x 10^{-20} cm^2)
$^4I_{9/2}$	11377	678.85	43.3	13.56	1.42
$^4I_{11/2}$	9452	738.54	47.1	19.32	3.80
$^4I_{13/2}$	7468	142.63	9.1	–	–
$^4I_{15/2}$	5324	6.89	0.5	–	–
		A_T (s^{-1}) $=1566.91 s^{-1}$		τ_R= 638 (μs)	

compares the spectroscopic quality factor (Ω_4/Ω_6) [47] and J-O intensity values in various hosts. The local structure and bonding around Ln^{3+} ions are revealed by the J-O parameter [42]. A significant value of Ω_2 indicates a strong covalency of the metal-ligand bonding, whereas a large value of Ω_6 indicates a high stiffness. The parameter Ω_2 is known to be structure/environment sensitive and to depend on the covalency and asymmetry of ion sites near Ln^{3+} ions, in contrast to Ω_6, which is dependent on vibronic effects [48]. Due to the nephelauxetic effect, covalent bonding reduces the electronic levels of free ions and raises Ω_2 values. It is found that for hypersensitive transitions with $|\Delta J| = 2$, Ω_2 becomes more significant [49]. The hosts' structural characteristics have a significant impact on the transitions' intensities.

3.8 Radiative properties from Ω_λ

The measured PL spectra of the fluorescence level $^4F_{3/2}$ of fixed Nd^{3+} doped alumino-silicate (SiNdAl3) glass are combined with phenomenological JO parameters calculated from absorption spectra in order to estimate various radiative values [50]. The emission cross-section of peaks [$\sigma_P(\lambda_P)$] between an initial manifold (ΨJ) and a terminal manifold ($\Psi' J'$) is used to determine these parameters [51].

$$\sigma_P(\lambda_P) = \frac{\lambda_P^4}{8\pi c n^2 \Delta\lambda_{eff}} A(\Psi J;\Psi' J') \quad (3)$$

Here, λ_P represents the maximum emission wavelength, $\Delta\lambda_{eff} = \frac{\int I(\lambda)d\lambda}{I_{max}}$ represents the effective bandwidth, and according to Table 7, $A(\Psi J;\Psi' J')$ represents the probability of emission for the specific transition. The radiative transition probability between the initial (ΨJ) and stimulated manifold ($\Psi' J'$) can only be calculated using the electric-dipole probability [50] and the average wavelength of the transition, as follows:

$$A_{ed}(\Psi J;\Psi' J') = \frac{64\pi^4 e^2 n(n^2+2)^2}{3h\lambda^3(2J+1)9} \Sigma_{\lambda=2,4,6}\Omega_\lambda(\Psi J\|U^\lambda\|\Psi' J')^2 \quad (4)$$

The total radiative probability (AS) is determined by summing the $A(\Psi J; \Psi' J')$ values for each state that takes part in the transition from the higher energy excited states (ΨJ) to the lower energy ground states ($\Psi' J'$) [51]. The radiative lifetime, which calculates the rate of population loss from a specific state, is the inverse of the total radiative probability (τ_R). Several transitions' branching ratios can written as:

$$\beta_r = \frac{A(\Psi J;\Psi' J')}{\sum A(\Psi J;\Psi' J')} \quad (5)$$

Calculations can be made to determine the radiative lifetime of an excited state ($\Psi' J'$):

$$\tau_R = \frac{1}{\Sigma A(\Psi J;\Psi' J')} \quad (6)$$

In Table 5, the relationships outlined in Eqs. 4–6 are employed to compute a range of radiative parameters for SiNdAl3 glass. Additionally, Table 8 presents a comparative analysis of laser characteristic parameter pertaining to Nd^{3+} ions across various glass systems for the $^4F_{3/2} \rightarrow {}^4I_{11/2}$ transition.

Table 8 Comparison of laser characteristic parameters of Nd^{3+} ions in different glass systems for the $^4F_{3/2} \rightarrow {}^4I_{11/2}$ transition

Glass	λ_P	$\Delta\lambda_{eff}$ (nm)	$\sigma_P(\lambda_P)$ (x 10^{-20} cm^2)	σ_P x $\Delta\lambda_{eff}$ (x 10^{-25} cm^2)
SiNdAl3 (Present work; annealed at 1060 °C)	1058	19.32	3.80	0.73
SPB1 [62]	1065	43	1.8	0.77
0.5NdGC [57]	1062	37.4	1.86	0.69
Glass F [63]	1063	39.98	1.66	0.61
Fluoride [64]	1058	30.6	1.87	0.57

3.9 Non-linear properties

The good optical quality of sol-gel SiO_2 glass is reflected in the non-linear refractive index (n_2), non-linear refractive index susceptibility ($\chi^{e(3)}$), coefficient (γ_{ce}), and suitably high Abbe number (υ_{Ab}) [52]. These non-linear qualities, which were determined from optical parameters, as described previously [52], are shown in Table 9. The disparities in the non-linear refractive index (n_2), susceptibility (χ) and coefficient (γ) of Nd^{3+} as influenced by diverse crystalline lattices are summarized in Table 10.

Table 9 Non-linear parameters of co-doped with SiNdAl3 in sol-gel glasses annealing at 1060 °C

n_f	n_e	n_f-n_e	n_d	υ_{Ab}	$1/\upsilon_{Ab}$	n_2 (10^{-13}esu)	γ (cm^2/W)	ω_o (*10^{-13})	N x 10^{-16}	χ x 10^{-7}
1.504	1.495	0.009	1.500	55.6	0.018	1.378	3.85	126.13	816.296	8.69

Table 10 Variations in the non-linear refractive index (n_2), susceptibility (χ) and coefficient (γ) of Nd^{3+} in different crystalline lattices

Glass	n_2 (10^{-13}esu)	χ x 10^{-7}	γ (cm^2/W)
SiNdAl3 (Present work; annealed at 1060 °C)	1.378	8.69	3.85
$Al(NO_3)_3$ [1]	1.351	–	3.684

4 Conclusions

The effect of Al doping on the photoluminescence properties of Nd3+ in silicate glass prepared by a sol-gel method are reported. Both Al co-doping and the annealing temperature have a significant impact on the PL intensity of Nd^{3+}. RE^{3+} ions are subjected to a modified vibrational coupling and RE^{3+} clustering is prevented by Al co-doping, and RE^{3+} are found in the aluminum-rich regions that have greater non-bringing Al-O groups available for coordination. The phonon energy of Al-O-Si bonds is lower than that of Si-O-Si bonds. XRD confirmed that the glass samples were amorphous. FTIR spectra showed that the sample annealed at higher temperatures had fewer the OH groups, together with NBO on the low phonon energy side. The JO intensities parameters are also estimated. The results indicate that an increase in Al concentrations strongly enhances the PL of the doped glasses. The branching ratio for $^4F_{3/2} \rightarrow {}^4I_{11/2}$ transition is larger than that of the $^4F_{3/2} \rightarrow {}^4I_{9/2}$ transition, which is usually true for Nd^{3+} doped laser materials. From the larger stimulated emission cross-section (3.80×10^{-20} cm^2) of the $^4F_{3/2} \rightarrow {}^4I_{11/2}$ transition, it is concluded that the SiNdAl glasses could be highly useful for the development of solid state laser material. Physical characteristics such as the relatively high Abbe number (ϑ_d), low non-linear refractive index (n_2), and non-linear susceptibility ($\chi^{e(3)}$) value confirm the sample's strong optical quality [53] and its superiority as a non-linear amorphous material.

Acknowledgements KMSD is thankful to Ministry of Tribal Affairs, Govt. of India for their financial support through NFST with Award letter 202122-NFST-MIZ-00237. We express their gratitude to the Department of Science and Technology, New Delhi (India) for their financial support under grant No. SR/S2/LOP-0039/2010.

Author contributions KMSD: Writing-Original draft preparation, Formal analysis, Investigation, Data curation, Visualization, Conceptualization, Writing-Reviewing and Editing, Methodology, Resources. Lp: Investigation. ALF: Investigation, Formal analysis. RL: Investigation SR: Investigation, Methodology, Resources, Conceptualization, Visualization, Review, Editing, Supervision.

Compliance with ethical standards

Conflict of interest The authors declare no competing interests.

Consent for publication The authors also declare the work is original and is not submitted or published anywhere.

References

1. Hazarika S, Rai S (2007) Characteristics of Nd^{3+} ions in sol-gel derived silicate glass in presence of $Al(NO_3)_3$ and the $^4F_{3/2} \rightarrow {}^4I_{11/2}$ transition. Opt Mater 30:462–467
2. Mohd A, Rai VK (2018) Study of visible luminescence spectra from Nd^{3+} doped TPO glass upon 808 nm excitation. AIP Conference Proc 1953:090048
3. Dawnglianaa KMS, Rai S (2023) Effect of titania nano composite on structural and optical properties of Ho^{3+} doped silica glasses for green laser applications. Appl Phys A 130:476
4. Soltys M, Pisarska J, Lesniak M, Sitarz M, Pisarski WA (2018) Structural and spectroscopic properties of lead phosphate glasses doubly doped with Tb^{3+} and Eu^{3+} ions. J Mol Struct 1163:418–427
5. Caldino U, Lira A, Meza RAN, Camarillo I, Lozada MR (2018) Development of sodium-zinc phosphate glasses doped with Dy^{3+}, Eu^{3+} and Dy^{3+}/ Eu^{3+} for yellow laser medium, reddish-orange and white phosphor applications. J Lumin 194:231–239
6. Kashif I, El-Maboud AA, Ratep A (2014) Effect of Nd_2O_3 addition on structure and characterization of lead bismuth borate glass. Results Phys 4:1–5
7. Pisarski WA, Kowalska K, Kuwik M, Polak J, Pietrasik E, Goryczka T, Pisarska J (2020) Novel multicomponent titanate-germanate glasses: synthesis, structure, properties, transition metal and rare earth doping. Mater 13(19):54–62
8. Ramesh P, Jagannath G, Eraiah B, Kokila MK (2018) Optical and physical investigations of lanthanum bismuth borate glasses doped with Ho_2O_3. Mater Sci Eng 310:012032
9. Venkateswarlu M, Mahamuda SK, Swapna K, Prasad MVVKS, Srinivasa Rao A, Mohan Babu A, Shakya S, Vijaya Prakash G (2015) Spectroscopic studies of Nd^{3+} doped lead tungsten tellurite glasses for the NIR emission at 1062 nm. Optical Mater 39:8–15
10. Snitzer E (1961) Optical maser action of Nd^{3+} in a barium crown glass. Phys Rev Lett 7:444
11. Yamane M, Asahara Y (2000) Glasses for Photonics, first ed., Cambridge University Press, UK
12. Silversmith AJ, Boye DM, Brewer KS, Gillespie CE, Lu Y, Campbell DL (2006) $^5D_3 \rightarrow {}^7F_J$ emission in terbium-doped sol–gel glasses. J Lumin 121:14–20
13. Bouzidi C, Ferhi M, Elhouichet H, Ferid M (2016) Structural and luminescence properties of $(Ba1-xEux)MoO_4$ powders. J Lum 179:230–235
14. Dabboussi S, Elhouichet H, Bouzidi C, Maliarevich GK, Gaponenko NV, Oueslati M (2009) Excitation and emission processes of Tb^{3+} in porous anodic alumina. J Appl Surface Sci 255:4255–4258

15. Almeida RM, Vasconcelos HC, Goncalves MC, Santos LF (1998) XPS and NEXAFS studies of rare-earth doped amorphous sol–gel films. J Non-Cryst Sol 232–234:65–71
16. Brinker CJ, Scherer GW, Roth EP (1985) Sol → gel → glass: II. Physical and structural evolution during constant heating rate experiments. J Non-Cryst Sol 72:345–368
17. Ferrari M, Piazza A, Montagna M, Carturan G, Campostrini R (1994) Site selection spectroscopy of SiO_2:Eu^{3+} gels. J Sol-Gel Sci Tech 2:783–786
18. Ferrari M, Campostrini R, Carturan G, Montagna M (1992) Spectroscopy of trivalent europium in gel-derived silica glasses. Philo Mag B 65:251–260
19. Zhu L, Zuo C (2010) Photoluminescence of Dy^{3+} and Sm^{3+}: SiO_2–Al_2O_3–LiF–CaF_2 glasses. Physica B: Cond Mat 405(21): 4401–4406
20. Arai K, Namikawa H, Kumata K, Honda T, Ishii Y, Handa T (1986) Aluminum or phosphorus co-doping effects on the fluorescence and structural properties of neodymium-doped silica glass. J App Phys 59:3430
21. Zhong H, Cai W, Zhang L (1999) Fluorescence properties of Tb^{3+} ions in SiO_2 glass co-doped with Al^{3+}. Mat Res Bul 34:233
22. Alombert- Goget G, Gaumer N, Obriot J, Rammal A, Chaussedent S, Monteil A, Portales H, Chiasera A, Ferrari M (2005) Aluminum effect on photoluminescence properties of sol–gel-derived Eu^{3+}-activated silicate glasses. J Non-Cryst Sol 351(21–23):1754–1758
23. Swapna K, Mahamuda SK (2014) Visible luminescence characteristics of Sm^{3+} doped Zinc Alumino Bismuth Borate glasses. J Lum 146:288–294
24. Kothari P (2014) Spectral and electrical studies of neodymium & erbium doped phosphate glasses. Inter E Publication
25. Bokatial L, Rai S (2012) Optical properties of Sm^{3+} ions in sol-gel derived alumino-silicate glasses. J Opt 41(2):94–103
26. Fneich H, Gaumer N, Gaumer N, Blanc W, Mehdi A (2018) Europium-doped sol-gel SiO_2-based glasses: effect of the europium source and content, magnesium addition and thermal treatment on their photoluminescence properties. Molecules 23:1768
27. Dawngliana KMS, Fanai AL, Lalruatpuia, Rai S (2022) Optical basicity and electronic polarizability of Sm^{3+}-doped silica glass prepared by sol-gel process. Materials Today: Proce 65: 2572–2577
28. Pascuta P, Pop L, Rada S, Bosca M, Culea E (2008) The local structure of bismuth borate glasses doped with europium ions evidenced by FT-IR spectroscopy. J Mat Sci Mat Elec 19:424
29. Rai S, Andrew LF (2016) Effect of the annealing and dopants concentration on the optical properties of Nd^{3+}:Al^{3+} co doped sol-gel silica glass. J Lum 170:325–329
30. Zamratul MIM, Zaidan AW, Khamirul AM, Nurzilla M, Halim SA (2016) Formation, structural and optical characterization of neodymium doped-zinc soda lime silica based glass. Results in Phys 6:295–298
31. Duhan S, Aghamkar P (2008) Synthesis and characterization of neodymium oxide in silica matrix by sol-gel protocol method. Res Lett Phys 237023:1–4
32. Zhang Y, Shan P, Zhang Z, Chen Z (2014) Growth, structure, thermal properties and spectroscopic characteristics of Nd-doped $KGdP_4O_{12}$ crystal. Pl One 9(6):1–10
33. Krishnia RR, Foob KY, Hameeda BH (2014) Adsorptive removal of methylene blue using the natural adsorbent-banana leaves. Desalination Water Treatment 52:6104–6112
34. Dawngliana KMS, Fanai AL, Rai S (2023) Structural and spectroscopic properties of Eu^{3+} ions in Alumino-Silicate glass. Indian J Pure & app Phys 60:1–8
35. Judd BR (1962) Optical absorption intensities of rare-earth ions. Phys Rev 127:750
36. Ofelt GS (1962) Intensities of crystal spectra of rare-earth ions. J Chem Phys 37:511
37. Carnall WT, Crosswhite H and Crosswhite HM (1978) Energy level structure and transition probabilities in the spectra of the trivalent lanthanides in LaF_3. Argonne National Laboratory, Report no. ANL-78-XX-95
38. Bhatia B, Meena SL, Parihar V, Poonia M (2015) Optical basicity and polarizability of Nd^{3+} doped bismuth borate glasses. New J Glass and Cere 5:44-52
39. Carnall WT, Fields PR, Rajnak KJ (1968) Electronic energy levels in the trivalent lanthanide aquo ions, I. Pr^{3+}, Nd^{3+}, Pm^{3+}, Sm^{3+}, Dy^{3+}, Ho^{3+}, Er^{3+}, and Tm^{3+}. Chem Phys 59:4424
40. Chimalawong P, Kaewkhao J, Kedkaew C, Limsuwan P (2010) Optical and electronic polarizability investigation of Nd^{3+}-doped soda-lime silicate glasses. J Phys Chem Sol 71:965–970
41. Dihingia PJ, Rai S (2012) Synthesis of TiO_2 nanoparticles and spectroscopic upconversion luminescence of Nd^{3+}-doped TiO_2–SiO_2 composite glass. J Lum 132:1243–1251
42. Sontakke AD, Annapurna K (2013) Spectroscopic properties and concentration effects on luminescence behavior of Nd^{3+} doped Zinc-Boro-Bismuthate glasses. Mat Chem Phys 137:916–921
43. Binnemans K, Gorller-Walrand C (1998) Are the Judd - Ofelt intensity parameters sensitive enough to reflect small compositional changes in lanthanide-doped glasses. J Phys Con Mat 10:167–170
44. Qiao Y, Da N, Chen D, Zhou Q, Qiu J, Akai T (2007) Spectroscopic properties of neodymium doped high silica glass and aluminum codoping effects on the enhancement of fluorescence emission. App. Phys. B 87:717–722
45. Reisfeld R, Panczer G, Patra A, Gaft M (1999) Time-resolved spectroscopy of Sm^{3+} in silica and silica–Al sol–gel glasses. Mater. Lett. 38:413–417
46. Syam Prasad P, Venkateswara Rao P (2018) Structural and Luminescence Properties of Tellurite Glasses for Laser Application. Mat Spr Cham 45:66
47. Jacobs RR, Weber MJ (1976) Dependence of the $^4F3/2 \rightarrow {}^4I_{11/2}$ induced-emission cross section for Nd^{3+} on glass composition. IEEE J Qua Elec 12:102
48. Singh G, Selvamani R (2017) Spectroscopic investigations of Nd^{3+} doped PLZT ceramics on the basis of Judd-Ofelt theory. J Lum 192:1084–1088
49. Hehlen MP, Brik MG, Kramer KW (2013) 50th anniversary of the Judd–Ofelt theory: An experimentalist's view of the formalism and its application. J Lum 136:221–239
50. Dawngliana KMS, Rai S (2022) Linear and nonlinear and Optical properties of Sm^{3+} co-doped alumino-silicate glass prepared by sol-gel method. J Non-Cryst Sol 598:121929
51. Chen B, Feng T (2021) J-O study of Nd-doped 8Y-ZrO_2 transparent ceramic and it potential application in infrared laser. J All Comp 884:161104
52. Dawngliana KMS, Fanai AL, Rai S (2023) Structural and optical studies of Sm^{3+}-doped silica glass along with TiO_2 nanoparticles for photonic applications. J Non-Cry Sol 607:122226
53. Burdick GW, Jayasankar CK, Richardson FS, Reid MF (1994) Energy-level and line-strength analysis of optical transitions between Stark levels in Nd^{3+}:$Y_3Al_5O_{12}$. Phys Rev B 50:16309
54. Wang SS, Zhou Y, Lam YL, Kam CH, Chan YC, Tao X (1997) Fabrication and characterization of neodymium-doped silica glass by sol-gel process. Mat Res Inn 1:92–96
55. Naveen Kumar K, Vijayalakshmi L, Ratnakaram YC (2015) Energy transfer based photoluminescence properties of (Sm^{3+}+Eu^{3+}):PEO + PVP polymer films for Red luminescent display device applications. Opt Mat 45:148–155
56. Rai S, Mandal B, Tiwari LB, Surya Thakur N (2023) Photoacoustic spectroscopy of some layered systems and Nd^{3+} and Gd^{3+} in oxides, Photoacoustic and Photothermal Spectroscopy. Prin App 23:263–279

57. Yu Y, Chen D, Ma E, Wang Y, Hu Z (2007) Spectroscopic properties of Nd^{3+} doped transparent oxyfluoride glass ceramics. Spectro Acta Part A 67:709–713
58. Mitra S, Jana S (2015) Properties of the energy bands, Judd-Ofelt parameters and the fluorescence of neodymium chloride ($NdCl_3$) in methanol, iso-propanol and butanol solvents. J Flu 25:541–549
59. Deopa N, Rao AS, Gupta M, Vijaya Prakash G (2018) Spectroscopic investigations of Nd^{3+} doped Lithium Lead Alumino Borate glasses for 1.06 μm laser applications. Opt Mat 75:127–134
60. Kesavulu CR, Kim HJ, Lee SW, Kaewkhao J, Wantana N, Kaewnuam E, Kothan S, Kaewjaeng S (2017) Spectroscopic investigations of Nd^{3+} doped gadolinium calcium silica borate glasses for the NIR emission at 1059 nm. J Alloys Comp 695:590–598
61. Choi JH, Margaryan A, Margaryan A, Shi FG (2005) Judd Ofelt analysis of spectroscopic properties of Nd^{3+}-doped novel fluorophosphates glass. J Lumin 114:167–177
62. Karthikeyan B, Philip R, Mohan S (2005) Optical and non-linear optical properties of Nd^{3+} doped heavy metal borate glasses. Opt Com 246:153–162
63. Deopa N, Rao AS, Gupta M, Vijaya Prakash G (2018) Spectroscopic investigations of Nd^{3+} doped Lithium Lead Alumino Borate glasses for 1.06 mm laser applications. Opt Mater 75:127–134
64. Florez A, Martinez JF, Florez M, Porcher P (2001) Optical transition probabilities and compositional dependence of Judd–Ofelt parameters of Nd^{3+} ions in fluoroindate glasses. J Non-Cryst Solids 284:261–267